Measurement 143 (2019) 267–275

Contents lists available at ScienceDirect

Measurement

journal homepage: www.elsevier.com/locate/measurement

An automated visual tracking measurement for quantifying wing and body motion of free-flying houseflies

Nazri Nasir *, Shabudin Mat

Department of Aeronautics, Automotive and Ocean Engineering, School of Mechanical Engineering, Faculty of Engineering, Universiti Teknologi Malaysia, 81310 Skudai, Johor, Malaysia

ARTICLE INFO

Article history:
Received 18 October 2017
Received in revised form 2 May 2019
Accepted 4 May 2019
Available online 10 May 2019

Keywords:
Camera
Housefly
Accuracy
Motion tracking

ABSTRACT

Pioneering discoveries revealed that flying insects actively regulate body appendages such as wings, legs and abdomen to stay aloft. However, the initial stage of capturing their motion during flight is rather challenging and time-consuming, especially during the digitization of lengthy video images. Therefore, our development of an automated visual tracking system will greatly provide a full access to insect's body and wing dynamics during flight. By using the positional dataset obtained from the digitized images which earlier captured by an automated time-resolved high-speed videography, we thus further three-dimensionally reconstructed body and wing dynamics of housefly *Musca domestica*. We validated and further compared the automated digitization with manual tracking. Our analysis estimates that motions along z-axis yields higher differences (16 ± 28.19 μm for thorax and 13 ± 99.19 μm for wingtip) because it orthogonally points to the cameras, which lead to acceptable inaccuracies of calibration coefficients due to the limited depth of focus.

1. Introduction

1.1. Overview

Insect flight is an inspiring feat of nature and for million years they evolved vast range of evolution. Hence, insect is a tool that widely used in genetics, animal physiology, ecology, evolutionary as well as aerodynamics. In general, insects are versatile during flight, lightweight structure and also small in size. Hence, insects were the pioneer creatures to take-off to the air and later observation confirmed that insect flight is essential for diverse activities. The detailed information of their body postures and wing motions especially during free flight displays vital indicator, evidences and proof for a conclusion.

The body and complex dynamic wing motion are greatly differ from fixed-wing aircraft, and these differences also explain flies' ability to lift them up to the air using comparatively small multi-purpose wing structure [1–3]. Unlike an airplane which uses fans to generate thrust, flies flap their flexible wings simultaneously to produce both lift and thrust [4,5]. Insect's wing motion consist of two translational (upstroke and downstroke) and another two rotational phases (supination and pronation), which always lead by the leading edge of the wings [6,7]. In general, flies imply different patterns of wing stroke and wingtip paths such as the figure of eight, distorted ellipse [8], with 1 (figure of eight), 2 [9] and 3 [10] crossing-overs. Previous data also shown that small insect performed "clap and fling" during dorsal stroke reversal [11,12]. These unique patterns of wing motion consequently lead to production of Leading Edge Vortex LEV, added mass, Magnus force, rotational circulation, delayed-stall mechanism and finally, wing-wake interactions. Using an appropriate wing motion, flies balance the body posture while simultaneously producing sufficient amount of vertical force to offset its weight (≈18.40 mg of total weight). Flies also actively adjust the dynamic coordination of other body appendages such as extension of legs (crickets [13], gliding ants [14], bees [15], birds [16], fruit flies [1]) and use the abdomen as a rudder [1,17].

1.2. Related works

Measuring insect body and wing kinematics is challenging because of fast flight speeds, small body size, fast changes in body postures, and structural deformations of body parts especially wing (e.g. spanwise bending [18], wing torsion [19] and cambering [20]). Many previous studies used tethered flight but this approach does not allow the studying of manoeuvre, change of body postures, unable essential sensory receptors and thus impairs the

* Corresponding author.
E-mail address: mnazri@mail.fkm.utm.my (N. Nasir).

https://doi.org/10.1016/j.measurement.2019.05.007
0263-2241/

Nomenclature

Symbols

α	Angle between the wing chord and vertical axis; wing angle of attack
β	Horizontal deviation angle between flight direction of the fly's centre of gravity and body yaw angle in global coordinate frame
ε	Angle between the flight path of an ascending fly and local horizon; body inclination
m	Mass
N	Number of flies
n	Wingbeat frequency measured when wing chord was perpendicular to stroke plane
Φ	Stroke angle of the wing with respect to fly's transversal body axis
θ	Elevation angle of the wing with respect to fly's longitudinal body axis
R^2	Coefficient of determination
r	Pearson's correlation coefficient
SSE	Sum of Squared Errors
u	Speed
V	Voltage
v	Velocity
η	Roll angle of the thorax with respect to fly's longitudinal body axis
ω	Yaw angle of fly's longitudinal axis about the vertical
χ	Pitch angle of fly's longitudinal axis with respect to horizon
ROI	Cameras' Region of Interest,
s.d.	Standard deviation
$()_a$	Airflow
$()_b$	Body
$()_h$	Horizontal
$()_v$	Vertical
$()_L$	Left
$()_R$	Right
$()_t$	Wingtip
$()_w$	Wing

feedback loop [21]. However, these problems can be resolved by numerous techniques of free-flight videography, which depend on experimental conditions. The simplest approach consists of mirrors and a single camera to capture multiple perspectives [22,23]. As the time goes on, more advanced approaches use multiple high-speed cameras to allow three-dimensional (3D) kinematic reconstruction as listed: (1) M*odel-based approach* uses image measurement of silhouettes, which matches with a model constructed separately [24,25]. This approach offers better accuracy for images containing obstructions, clutters, poor contrast, low-lighting environment and can accurately estimate structural appearances. (2) *Reconstruction-based approach*, on the other hand, does not require any preceding model [26,27]. Body parts and wings are marked with fluorescent markers as previously used in other applications [28,29], linked by connecting lines to approximate shape of the moving structures. However, in this approach, the accuracy of reconstruction depends on structural deformations of body and wings.

1.3. Contribution of the paper

In the present study, we proposed an automated visual tracking measurement for quantifying a complete description of wing and body motion in free-flying houseflies, *Musca domestica* (see Fig. 1) using *reconstruction-based approach*. We first measured the morphological data and further analysed the time course of detailed body and wings kinematics of housefly during free flight under laboratory condition. Finally, we performed accuracy assessment and measurement uncertainty in order to validate the results of automated tracked positional data with manually tracking.

2. Material and methods

2.1. Animal

Flies were reared at the Department of Neurobiology, University of Ulm, Germany. Nearly 30-40 flies were kept on a 16:8-h (light:-dark) cycle, inside a transparent glass enclosure (50 cm × 30 cm × 30 cm) with sugar cubes and water as their nutrition. In all experiments, I used 5–10 days old wild type female houseflies. The animal are shown to scale (model AT21 Comparator microgram balance, Mettler Toledo International Inc., Greifensee, Switzerland), wet body mass, m_b was 18.39 ± 2.02 mg (mean ± s.d, N = 10) and wet translucent wing mass, m_w taken as 8.32 ± 52.32 μg. Body length was 9.62 ± 0.02 mm and wing length 6.98 ± 0.03 mm. Before the experiment, I pre-selected up to 4 flies using a white light trap placed at the enclosure's ceiling, thus attracted active and flyable flies.

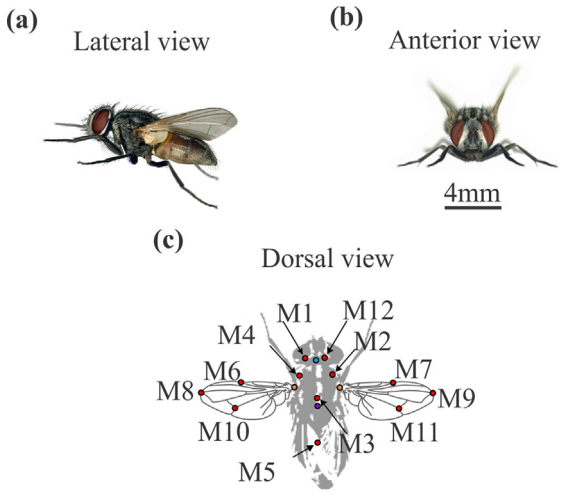

Fig. 1. Morphology of a housefly (Hastings et al. 2004, see Table 1: Position of markers). The virtual markers formulated from fly's morphology are the centre of gravity (purple dot), centre of head rotation (cyan dot) and the wing hinges (orange dots). (For interpretation of the references to colour in this figure legend, the reader is referred to the web version of this article.)

2.2. Marking procedure

The flies were anesthetized for 4 min on ice flakes (2–4 °C) before I marked them with 12 fluorescent dots (Pedeko, Monchengladbach, Germany; Fig. 1c) on their head (2 markers), thorax (3 markers), abdomen (1 marker), and both wings (6 markers). It took approximately 5 minutes and every marker had an average mass of 0.1 μg to prevent wing deformation due to inertia. The average size of each dot was 0.25 mm (3–5 video pixels) in diameter. After that, the flies were taken to the take-off platform and they were allowed to recover (Fig. 2a). To guide the animal

Table 1
Position of markers.

Marker	Position
1	In between compound eyes and postocular state
2	Right presutural setae
3	Dorsal thorax, in front of scutellum
4	Left presutural setae
5	Dorsal abdomen at the centre of tegite 4
6	Left leading edge of the wings, which connect vein R1 and end of vein C
7	Right leading edge of the wings, which connect vein R1 and end of vein C
8	Left wingtips, which connect vein C and end of vein R4+5, vein M
9	Right wingtips, which connect vein C and end of vein R4+5, vein M
10	Left wing, which connect vein CuA1 and end of vein dm-cu
11	Right wing, which connect vein CuA1 and end of vein dm-cu
12	In between postocular state and compound eyes

during vertical take-off, I mounted three white LEDs (5 mm diameter, Cree, NC, US) around the casing of phototransistor.

2.3. Videography

To film the fluorescent markers, I built up a modified experimental setup similar to the previously used approaches using master-slave configuration [26,30]. The experimental setup consists of three high-speed cameras (6000 frames per second, 1280 × 800-pixel resolution, model Phantom v12, Vision Research Inc., Wayne, NJ, USA; Fig. 2a-b) and calibrated using Direct Linear Transformation [31]. At 170 Hz average wingbeat frequency, this resulted a temporal resolution of 35.3 video frames per wing stroke cycle. The cameras were mounted with an inter-camera angle of 120°, 18 cm above the arena that allowed me to track flies inside a fields of view of 6 cm × 5 cm × 5 cm (length × width × height).

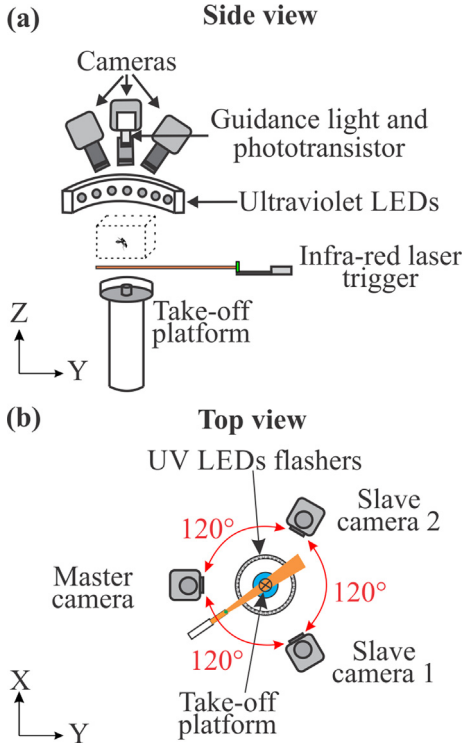

Fig. 2. Experimental setup of 3D-videography to record flight of freely flying flies. (a) The arrangement of high-speed cameras (Phantom v12) and ultraviolet (UV) LED flashers placed on top of the cameras' Region of Interest, ROI. White guidance LEDs light provides visual guidance (5 mm diameter, Cree, NC, US). (b) Top view of the experimental setup.

Each camera was equipped with microlenses (Nikkor, 60 mm, f/2.8D, Nikon, Japan) that fitted with ultraviolet and light-red filters (Jos. Schneider Optische Werke GmbH, Bad Kreuznach, Germany) to sieve out the light reflected by the fluorescent markers.

2.4. Airflow condition

The cameras' Region of Interest, ROI is not a closed volume, thereby, might be contaminated by flow from outside the experimental setup. I thus measured the ambient airspeed at the centre of ROI for 100 s using a tiny heated-bead thermistor (model 111-202CAK-H01, 0.36 mm diameter, 0.5 s time constant in air, 25 kHz sampling rate, Honeywell, NJ, US), whose electrical resistance depends on temperature, thus on fluid velocity. The data were logged by a 4-channel digital oscilloscope (model TDS3034B, 300 MHz Tektronix Inc., OR, USA) synchronized by the trigger from the master camera. To convert the thermistor voltage to airspeed, I used a commercial thermal anemometer (model TA5, Airflow Lufttechnik GmbH, Rheinbach, Germany). This procedure yielded a relationship between airspeed, u_a and measured voltage, V, which is expressed as the exponential calibration curve, u_a (Goodness of fit: SSE = 880.4×10^{-6}, $R^2 = 0.99$):

$$u_a = 60.52e^{-\left(\frac{V-11.82}{4.03}\right)^2} + 0.61e^{-\left(\frac{V-3}{1.86}\right)^2} \quad (1)$$

Under this measurement, the ambient airspeed was only 0.07 ± 0.01 ms^{-1} (mean ± s.d.).

2.5. Ultraviolet light flasher

To reduce motion blur of fluorescent markers on the captured videos, a ring of 40 ultraviolet light emitting diodes, UV LEDs (3 mm diameter, 405 nm wavelength, 40 mW sr^{-1} radiant intensity, 20° viewing angle, Bivar, CA, US) were flashed with 60 µs light pulses and synchronized with cameras (Fig. 2a-b). The UV LEDs were attached around a black-coated aluminium ring by using heat resistant epoxy. This configuration distributed ultraviolet light to all directions which is beneficial to record the fly's manoeuvres even during extreme inclination of body angle. Mean brightness of ROI due to the ultraviolet and guidance lights were 9 ± 5% lux (mean ± s.d.). Although ultraviolet light illumination caused degradation in performance during flight, flies were still capable to actively perform the visual task given [30].

2.6. Optical detection system

To record images immediately when the fly is in the ROI, I prepared an optical detection system to automatically trigger the cameras [32]. I constructed a light path employing a horizontally oriented 2 mm thickness infrared laser sheet (model QL8516SA, 850 nm wavelength, 60° opening angle, 30 mW, 5.6 mm diameter, driven by EU-37 SMD laser diode driver, Roithner Lasertechnik GmbH, Vienna, Austria). At the same time, a phototransistor above the arena (model L-53P3C, Kingbright, Taiwan, stored inside a cylindrical custom-made PVC housing) perceived changes in laser light when the fly crossed the sheet. A CCD zoom lens (model TF15DA-8, 1/3 Inch CCD 15 mm, f/2.2 fixed focal length manual Iris C-mount, Fujinon, Tokyo, Japan) fitted with an infrared filter (830 nm infrared filter, model R-72, Heliopan Lichtfilter-Technik Summer GmbH & Co KG, Munich, Germany) was attached in front of the phototransistor's housing. Whenever a fly crossed the laser sheet, the phototransistor which connected to a custom-made switching circuit, transmitted a 5 V transistor-transistor logic, TTL signal to a data acquisition system (14-Bits, 48 kS/s, NI USB 6009, National Instruments, TX, USA). The TTL signal was then further transmitted to a computer (Acer EXTENSA E264 E5200,

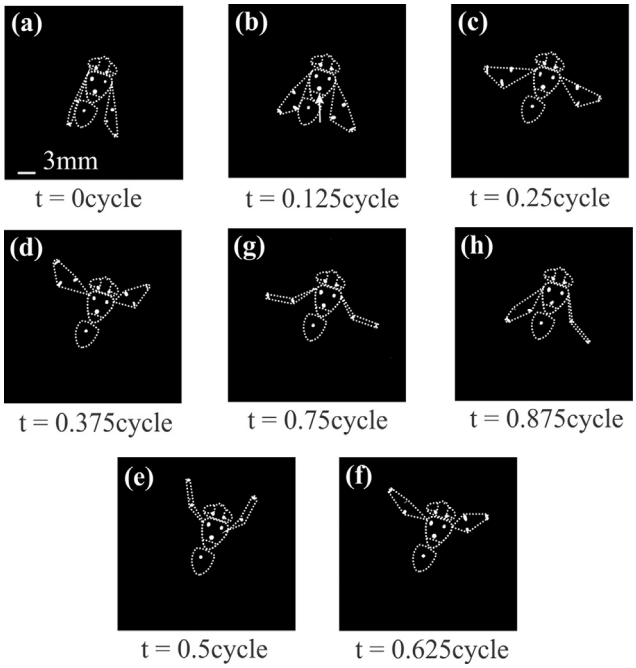

Fig. 3. Series Timeline of raw images filmed from a master camera. The raw images show a representative housefly during take-off (wing stroke period of 6 ms). Dotted lines depict fly body and wings.

3.20 GHz Inter® Core™) and the master camera. The fly's photoreceptors could not sense the infrared laser sheet because the visual sensitivity of the photoreceptors ranges from 380 to 600 nm [33].

2.7. Image processing and three-dimensional reconstruction

To improve image quality and eliminate noises, I used the software VirtualDub v1.9.9 ([34]; Fig. 3. The image processing tool stretched the brightness level according to image histogram ([0.00–0.023] > 2.01 > [0.00–1.00] (Y)), increased the contrast (400%), and applied box blur (radius 2, power 2). These procedures enhanced the automated position tracking and kept the adjusted search window at the centre of markers.

The ROI was calibrated using "millimeter graph paper" that was visible on all cameras. There are 25 positions of calibration point in eight different layers of 5 mm equidistant steps in height, resulting in a total of 200 positions inside the ROI (Fig. 2a). I repeated the calibration procedures several times before and after the experiments are performed to ensure high accuracy and consistency.

For marker tracking and digitizing, I used a software algorithm MATLAB™ v7 (The MathWorks, Natick, MA, USA) named DLTdv3 [26]. This application has a helpful graphical user interface such as zooming, auto tracking mode, real-time viewing of different cameras at the same window with 95% confidence intervals. The auto-tracker attempts to anticipate the location of specific markers on successive video frames by fitting an equation to previously digitized markers and extrapolating the position. During automated digitization, I used a linear Kalman filter as a fitting equation to predict the location of the subsequent frame. If predicted markers position matched to a specific auto track threshold, the auto tracker proceeded to examine the next frame. The software uses images from at least two cameras and the appropriate DLT coefficients to reconstruct the three-dimensional body and wings' motions. The tracking algorithm processed one image in 0.15 s on a 3.20 GHz Inter® Core™ computer.

The algorithms for body and wing motion reconstructions were adopted from previous scripts [32] with a few amendments on fly size and morphology. I further expanded the measured markers by a set of virtual body markers that were reconstructed from the fly's morphology. I estimated the position of centre of gravity, and centre of head rotation with respect to markers measured on the thorax from anatomical drawings [35]. The longitudinal body axis (anteroposterior axis) connects the centre of head rotation (near cervix) with the centre of gravity. The transversal body axis (also known as lateral axis) passes through the thorax and connects both wing hinges. These two axes define the thorax horizontal plane. Meanwhile, the thorax vertical axis (dorsoventral axis) point is normal to the thorax horizontal plane. See supplementary material for movies of an exemplary reconstruction of flight sequence (Fig. 4, Movie 1).

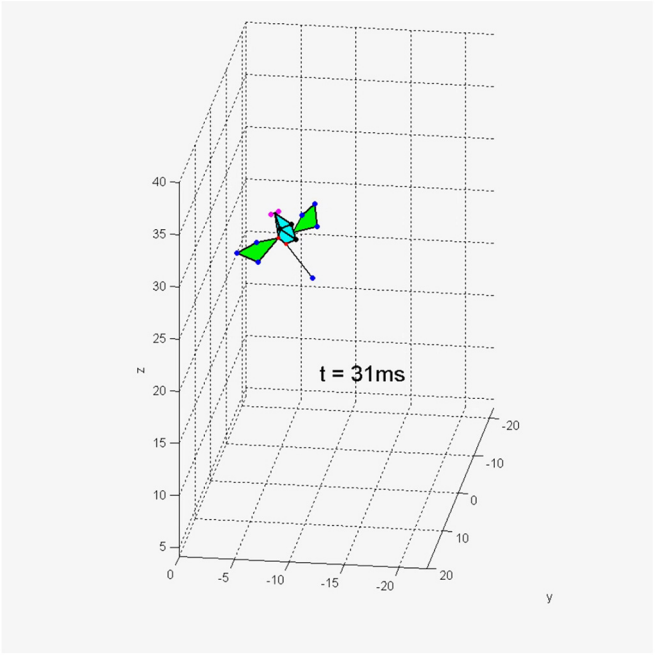

Movie 1.

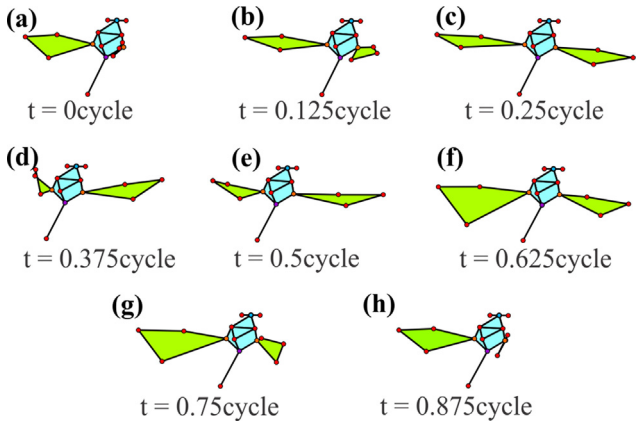

Fig. 4. 3D reconstruction of wings and body motion during free flight. See supplementary material for movies of an exemplary reconstruction of flight sequence (Movie 1).

The coordinate transformation from global coordinates to body-centred coordinate systems followed Haslwanter approach [36]. Global coordinate systems are typically used to evaluate flight trajectories whereas body-centred coordinate systems are used to score kinematic parameters of the animal [37]. Position in the body-centred coordinate system estimated from global coordinates by subtracting the position of fly's centre of gravity in each time step from the positions of all markers in that time step.

From this coordinate transformation, I further calculated other flight parameters such as body yaw ω (body rotation about dorsoventral axis), pitch χ (body rotation about transversal axis), and roll η (body rotation about longitudinal axis) angle (Fig. 8b-c). The wing kinematic parameters are wing stroke angle Φ (which is defined by the angle between wing rotational axis and transversal body axis), wing elevation angle θ (which is defined by the angle between wing rotational axis and wing stroke plane), and wing angle of attack α (which is defined by angle between the wing chord and the vertical axis (in global coordinate system; Fig. 9b-c). See for a complete time trace of exemplary flight sequence.

3. Results and discussion

Errors are commonly arising because of inaccurate calibration coefficient, tracking error, highly rolled or pitched body orientation, blocked by other body parts and also due to optical distortion [38,39]. Digitization error affects both the accuracy and reliability of extracted position measurements [40,41]. Thus, these errors should be carefully measured and further issues realistic confidence interval. To investigate position tracking performance and accuracy, I compared manual digitization with automated tracking procedures of marker 2 positioned on fly's thorax and marker 8 positioned on fly's left wingtip for 300 frames during extreme ascending flight maneuver (50 ms of recording time; Fig. 1c). Markers 2 located on fly's membranous thorax structure merely subjected to steady translational motion and rotation along three body axes. Compared to markers painted on flies' thoracic exoskeleton, markers 8 which placed at the wing tip, not only experienced body translation, but also unique combination of wing flapping, rotation and elevation throughout the stroke. Therefore, this highly flexible wing motion has subjected to chordwise wing deformation, bending and torsion which presumably will tremendously affect the tracking performance.

3.1. Quantifying tracking performance on the fly's body

I quantified the changes in accuracy between the coordinates extracted by each method using histograms of residuals as proposed by the previous studies [24,39]. The positional differences of marker 2 between automated and manual tracking ($X/Y/Z_{human\ digitization} - X/Y/Z_{automated\ tracking}$) are plotted including histograms of residuals (Fig. 5). The differences present in mean ± s.d. are: 4.16 ± 10.35 μm (median = 4 μm, X-axis), −1.13 ± 10.23 μm (median = −0.59 μm, Y-axis), 16 ± 28.19 μm (median = 13.15 μm, Z-axis). The differences are the smallest in the x-y plane because both axes are in the same plane of focus. By contrast, Z-axis yields higher differences because it orthogonally points to the cameras, which may lead to inaccuracies of calibration coefficients due to the limited depth of focus. These inaccuracies in position measurements caused by calibration error occur both in automated and human tracking. However, Kalman filter as predictive tracking algorithm provided in automated tracking software improves the tracking accuracy.

3.2. Quantifying tracking performance on the fly's wing

Positional differences of marker 8 between both tracking approaches are shown in Fig. 6. The mean ± s.d. differences are: 16.46 ± 116.98 μm (median = 0.73 μm, at X-axis), −11.42 ± 70.01 μm (median = −0.4 μm, at Y-axis) and 13 ± 99.19 μm (median =

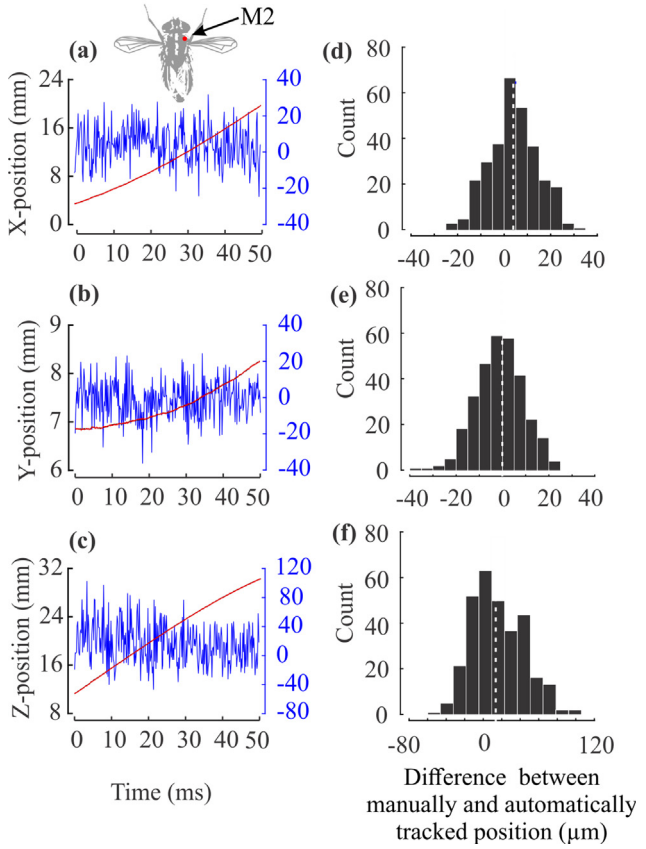

Fig. 5. Comparison between manual and automatic tracking precision of fluorescent marker 2 (located on the thorax), at (a) X-axis, (b) Y-axis and (c) Z-axis. Black dashed lines are positions of manually tracked data while the red line represents positional data of automatic tracker (left scale). Blue solid line shows the dissimilarities between manual and automatic position tracking (right scale). (d–f) Histogram of residuals and its medians (dotted white lines). (For interpretation of the references to colour in this figure legend, the reader is referred to the web version of this article).

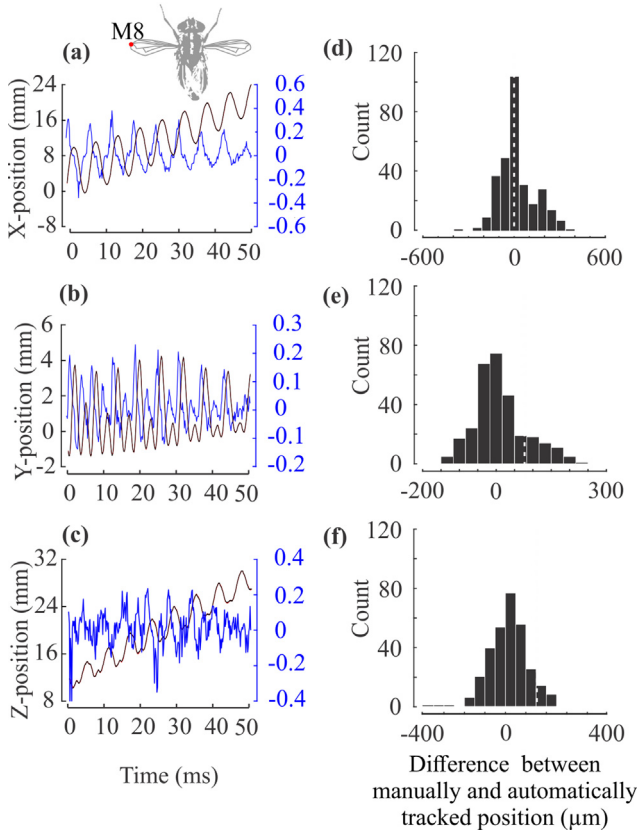

Fig. 6. Comparison between manual and automatic tracking precision of fluorescent marker 8 (located on the left wing), at (a) X-axis, (b) Y-axis and (c) Z-axis. Black dashed lines are positions of manually tracked data while solid red line depicts positional data of automatic tracker (left scale). The blue line shows the dissimilarities between manual and automatic position tracking (right scale). (d–f) Histogram of residuals and its medians (dotted white lines). (For interpretation of the references to colour in this figure legend, the reader is referred to the web version of this article).

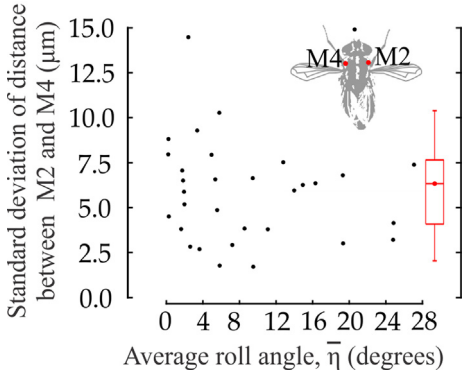

Fig. 7. Evaluation of tracking accuracy due to an extreme inclination of body angle. Data demonstrate the standard deviation of ground distance between marker 2 and 4 (located on the thorax) of 32 flies. The box plot represents mean, median and distribution of standard deviation of all measured flight sequences.

17.07 μm, at Z-axis), respectively. The differences increase at mid-stroke of the wing flapping cycle because wing translates at maximum speed. Moreover, elevated wing translational velocities cause motion blur, which turns round markers into oval and stretched markers. In this case, crosshairs provided by the software to assist in locating the moving markers of interest often failed. In both approaches, angular errors of wing motion caused by the

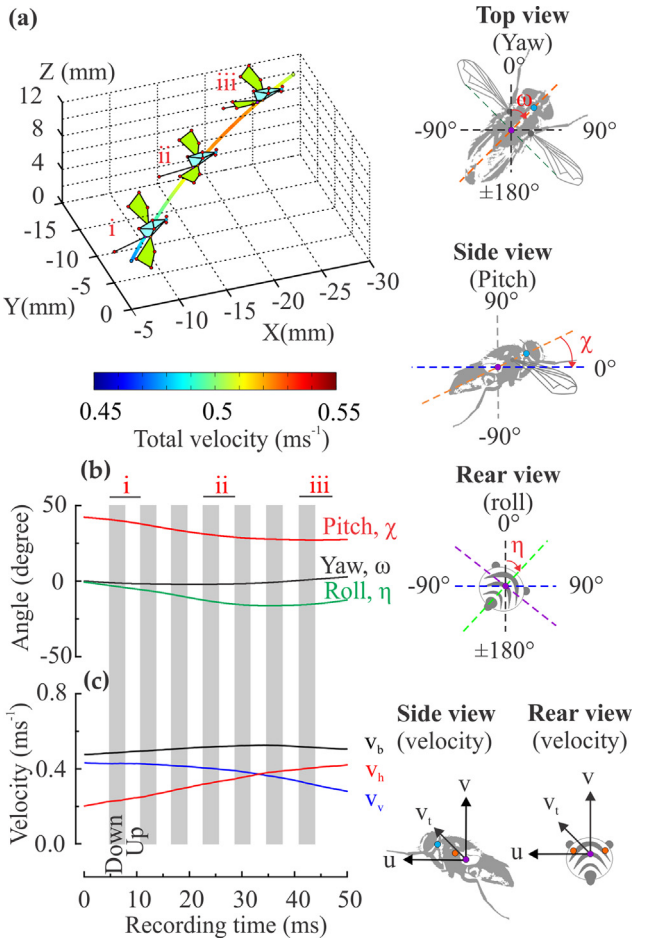

Fig. 8. Timelines of a 50 ms of body motion during flight. (a) 3D flight trajectory of a housefly at 6.38 ms (i), 24.14 ms (ii), and 42.12 ms (iii) after take-off maneuver. Body velocities of centre of mass are plotted in pseudo-colour. (b) Body angles (yaw, pitch, and roll). (c) Body vertical translational velocity, V_v (blue), body horizontal translational velocity, V_h (red) and total body translational velocity, V_b (black) throughout the flight sequence. (For interpretation of the references to colour in this figure legend, the reader is referred to the web version of this article).

measured positional differences were less than ~0.14°, which is acceptable. Presumably, there are additional errors in the method used due to wing structural deformation, ancestral inaccuracy and inaccuracy in morphological measurement. Hence, the similarity of results obtained by automated tracking software and manual tracking program confirmed that both methods are capturing the wing and body motion within an acceptable level of accuracy. Collectively, the results indicate that the proposed method is an accurate method with very low inaccuracies for the motion videography of fast moving creatures.

3.3. Positional error during high degree of body rotation

To further assess the significance of positional errors on a high degree of body orientation and postures (e.g. extreme body roll or body pitch), I estimated distance between markers 2 and 4 on the thorax of 32 flies with different average roll angle (Fig. 7). Measurement errors owing to excessive body rotation occur because cameras that are orthogonally mounted with respect to ROI capture round fluorescence markers as oval blobs. The associated imprecision are displayed concisely as the standard deviation of measured distance of a flight sequence. In all examined body orientations, there is no apparent relationship between the standard deviation of the measured distance when body roll increases

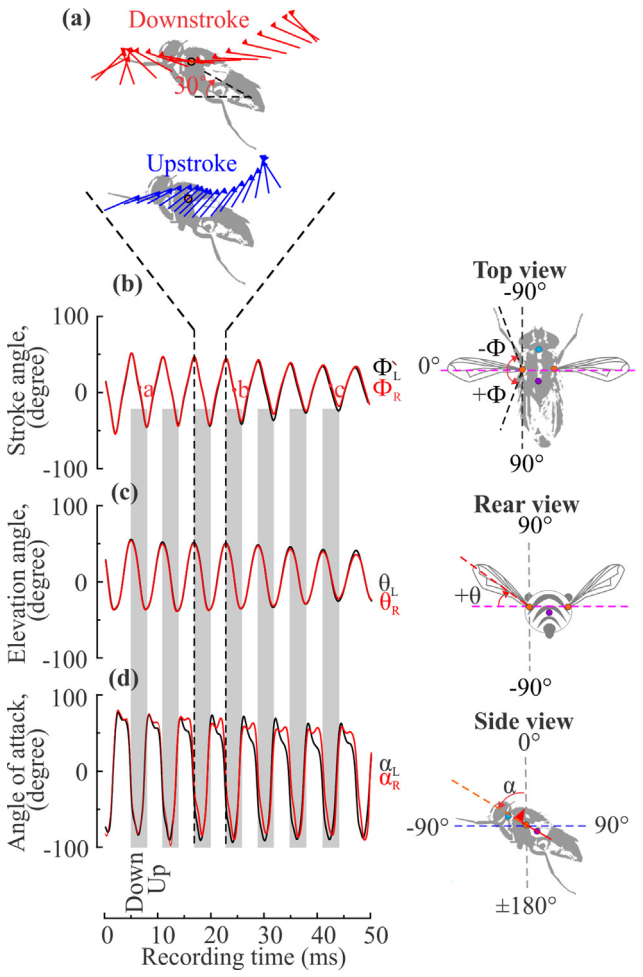

Fig. 9. Timelines of a 50 ms of wings motion during flight. (b) Wing stroke angle, Φ; (c) wing elevation angle, θ; (d) wing angle of attack, α; (a) wing motion during upstroke (blue) and downstroke (red). For this representative flight sequence, wingbeat amplitude was 89°, angle of attack at mid-stroke were 59° during supination and −84° during pronation and wingbeat frequency was 167 Hz. Red triangles indicate leading edges of the wing, and the body was pitched at 30° with respect to horizontal. (For interpretation of the references to colour in this figure legend, the reader is referred to the web version of this article).

(Pearson's coefficient, r = −0.02). Mean standard deviation of the distances for 32 flight sequences is 6.09 ± 3.15 μm (mean ± s.d.), which is relatively small, even at a high inclination of the thoracic structure. Tracking precision presumably can be enhanced by slightly tilting and mounting the cameras with 120° inter-camera angle as shown in Fig. 2a-b. Overall, we show that these errors are relatively small compared to body size and have no systematic dependencies.

3.4. Exemplary flight sequence

In order to show the utility of the proposed method, we apply it to a recorded maneuver that demonstrate how insects perform flight Fig. 8 (body motion) and Fig. 9 (wing motion) shows the pseudo-colour coded flight path of an exemplary fly during climbing flight.

After take-off from the platform, flies flew on average with 0.36 ± 0.1 ms^{-1} of vertical translational velocity, which is higher than horizontal translational velocity (0.23 ± 0.1 ms^{-1}, N = 32). Initially, flies flew upward with 0.39 ± 0.12 ms^{-1} before gradually exhibited vertical deceleration when they approached a transition from predominant vertical to horizontal flight manoeuvres. In general, flies first initiated flight with a steep increase of angular pitch velocity (pitch-up acceleration, 18378 ± 89 s^{-2}, N = 32). When flies reached a steady flight condition with predominant horizontal translational motion, they gradually decelerated their angular body pitch (nose-down, −41556 ± 140 s^{-2}, N = 32) presumably due to drag acting on the ventral body surfaces. Pitching moment depends on body angle and vary throughout the stroke cycle due to the change of stroke angle [42]. It predominately depends on changes in the mean vertical force of both wings at the stroke reversals [43]. Dorsal stroke reversal should have a higher effect on body pitch control because of the asymmetries in stroke angle and the moment arm is longer at this time of the stroke cycle compared to the ventral stroke reversal. In contrast, the change in body roll angle was however relatively minimal (mean, 7.25 ± 1.26°, N = 32).

The wing flaps up (backward) and downstroke (frontward) in between dorsal and ventral stroke reversal, which simultaneously rotates around leading edge or also known as span axis. According to the exemplary banana-shaped wing stroke trajectory, the left and right wing flap symmetrically with relatively higher wingbeat amplitude and later gradually decline as flies achieve stable flight (rate of decline −2068.50 s^{-1} in left wing and −2040.79 s^{-1} in right wing, correlation analysis between wingtip velocity and time, r_{left} = 0.95 and r_{right} = 0.98). The unstable flight condition perhaps, occurred due to instabilities introduced by the jumping during flight initiation [44]. Flies, mostly performed flight at wingbeat amplitude of 84.5 ± 3.4° (46 ± 3.4° stroke angle at dorsal reversal and −38.4 ± 3.8° stroke angle at ventral reversal) and mean wing elevation amplitude of 80.2 ± 5.1° (51.5 ± 1.8° elevation angle at dorsal reversal, −28.7 ± 4.4° elevation angle at ventral reversal). Strokewise-averaged wingtip velocity was 3.9 ± 0.1 ms^{-1} and strokewise-averaged wing angle of attack 63 ± 5.4° during the upstroke and −41.6 ± 6° during the downstroke. In consistent with previous finding [44], the fly does not performed clap and fling which presumably due to the artifact of tethering [5].

4. Conclusion

In this paper, we proposed a three-dimensional automated visual tracking device for fast moving creatures that has robustness in term of the tracking performance. The current state advancement of tracking framework associated with optical detection system definitely reduce the labour-intensive nature due to manual digitization and eliminated inconsistency attributed by inexperience human tracking technique. The proposed tracking method has much lower processing time with relatively adequate and comparable level of accuracy with a human visual inspection. Our method also offers a promise of capability to analyse much larger and lengthier video of flight sequences. Finally, the proposed method is a general-purpose approach which is adaptable and also ready to be modified for other forms of locomotion.

The application of the method adds substantially new insight into understanding of complex dynamics body and wing motion for flight control, particularly during free flight. Compared with the previous approach [45], our proposed method resolves the roll and pitch of the body well, even at extreme body orientations. Eventually, the effect of body posture and wing motion manifest themselves through the production of aerodynamic forces. A correct dataset of body postures and wing kinematics are useful input to computation of fluid forces using semi-empirical unsteady blade element (USBE) model [18], computational fluid dynamics (CFD) analysis [46,47], and a physical robotic wing experiment [42,48].

My current study also able to compute wing deformation which prominent in larger insects because the extracted painted and virtual markers are adequate to estimate structural deformation

including wing camber [49], torsional compliance [50] and spanwise deformation [18]. By having a complete package of body and wing motion, elaborate structural deformation and forces may lead to a new field of study on dynamics fluid-structure interaction and aeroelasticity. This research also accommodates a basis for future research on control and stability during the flight of natural fliers including biomimetic flying machines. Within the last decade, there was considerable progress in the development of bio-inspired Micro Aerial Vehicles MAV designed by engineers and physicist [51–55]. I hope that the ideas and findings of this inter-disciplinary studies will help engineers and biologists to enhance their understanding of insect flight [24].

Acknowledgements

This work was funded by a scholarship awarded by Universiti Teknologi Malaysia (UTM) to N.N. and grant Potential Academic Staff (PAS; Grant number: PY/2017/01068) financed this work. This research was also supported by UTM Aeronautics Laboratory (Aerolab). Most of the data and information included in this research article were extracted from N.N.'s thesis. This work was assisted by grants LE905/9-3 and LE905/10-1 of the German Science Foundation. We would like to thank Sarah Azreen Muhamad for critically reading the manuscript and the referees for their constructive comments.

References

[1] R. Berthé, F.-O. Lehmann, Body appendages fine-tune posture and moments in freely manoeuvring fruit flies, J. Exp. Biol. 20 (218) (2015) 3295, https://doi.org/10.1242/jeb.122408.
[2] S.A. Combes, T.L. Daniel, Flexural stiffness in insect wings II. Spatial distribution and dynamic wing bending, J. Exp. Biol. 17 (206) (2003) 2989, https://doi.org/10.1242/jeb.00524.
[3] J. Iriarte-Díaz, D.K. Riskin, D.J. Willis, K.S. Breuer, S.M. Swartz, Whole-body kinematics of a fruit bat reveal the influence of wing inertia on body accelerations, J. Exp. Biol. 9 (214) (2011) 1546, https://doi.org/10.1242/jeb.037804.
[4] S. Dalton, Borne on the Wind: Extraordinary World of Insects in Flight, Reader's Digest Press, 1975.
[5] S.N. Fry, R. Sayaman, M.H. Dickinson, The aerodynamics of hovering flight in Drosophila, J. Exp. Biol. 12 (208) (2005) 2303, https://doi.org/10.1242/jeb.01612.
[6] D.D. Chin, D. Lentink, Flapping wing aerodynamics: from insects to vertebrates, J. Exp. Biol. 7 (219) (2016) 920, https://doi.org/10.1242/jeb.042317.
[7] M.H. Dickinson, F.-O. Lehmann, S.P. Sane, Wing rotation and the aerodynamic basis of insect flight, Science (New York, N.Y.) 5422 (284) (1999) 1954.
[8] F.S.J. Hollick, The flight of the dipterous fly Muscina stabulans fallen, Philos. Trans. Roy. Soc. Lond. B 572 (230) (1940) 357, https://doi.org/10.1098/rstb.1940.0003.
[9] C.P. Ellington, The aerodynamics of hovering insect flight. III. Kinematics, Philos. Trans. Roy. Soc. Lond. B 1122 (305) (1984) 41, https://doi.org/10.1098/rstb.1984.0051.
[10] W. Neuhaus, R. Wohlgemuth, Über das Fächeln der Bienen und dessen Verhältnis zum Fliegen, Zeitschrift fur Vergleichende Physiol. (43) (1960) 615–641.
[11] X. Cheng, M. Sun, Wing-kinematics measurement and aerodynamics in a small insect in hovering flight, Nature 6 (2016) 25706, https://doi.org/10.1038/srep25706.
[12] L.A. Miller, C.S. Peskin, A computational fluid dynamics of 'clap and fling' in the smallest insects, J. Exp. Biol. 2 (208) (2005) 195, https://doi.org/10.1242/jeb.01376.
[13] M.L. May, R.R. Hoy, Leg-induced steering in flying crickets, J. Exp. Biol. 1 (151) (1990) 485.
[14] S.P. Yanoviak, Y. Munk, M. Kaspari, R. Dudley, Aerial manoeuvrability in wingless gliding ants (Cephalotes atratus), Proc. R. Soc. Lond. B 1691 (277) (2010) 2199, https://doi.org/10.1098/rspb.2010.0170.
[15] S.A. Combes, R. Dudley, Turbulence-driven instabilities limit insect flight performance, Proc. Natl. Acad. Sci.e USA 22 (106) (2009) 9105, https://doi.org/10.1073/pnas.0902186106.
[16] C.J. Pennycuick, A wind-tunnel study of gliding flight in the pigeon Columba Livia, J. Exp. Biol. 3 (49) (1968) 509.
[17] B.H. Dickerson, Z.N. Aldworth, T.L. Daniel, Control of moth flight posture is mediated by wing mechanosensory feedback, J. Exp. Biol. 13 (217) (2014) 2301, https://doi.org/10.1242/jeb.103770.
[18] F.-O. Lehmann, S. Gorb, N. Nasir, P. Schützner, Elastic deformation and energy loss of flapping fly wings, J. Exp. Biol. 17 (214) (2011) 2949, https://doi.org/10.1242/jeb.045351.
[19] R.J. Wootton, R.C. Herbert, P.G. Young, K.E. Evans, Approaches to the structural modelling of insect wings, Philos. Trans. Roy. Soc. Lond. B 1437 (358) (2003) 1577, https://doi.org/10.1098/rstb.2003.1351.
[20] A.R. Ennos, The inertial cause of wing rotation in Diptera, J. Exp. Biol. 1 (140) (1988) 161.
[21] M.H. Dickinson, F.-O. Lehmann, K.G. Götz, The active control of wing rotation by Drosophila, J. Exp. Biol. 1 (182) (1993) 173.
[22] R.J. Bomphrey, S.M. Walker, G.K. Taylor, The typical flight performance of blowflies: measuring the normal performance envelope of Calliphora vicina using a novel corner-cube arena, PLoS ONE 11 (4) (2009), https://doi.org/10.1371/journal.pone.0007852 e7852.
[23] B.W. Tobalske, D.R. Warrick, C.J. Clark, D.R. Powers, T.L. Hedrick, G.A. Hyder, A. A. Biewener, Three-dimensional kinematics of hummingbird flight, J. Exp. Biol. Pt 13 (210) (2007) 2368, https://doi.org/10.1242/jeb.005686.
[24] S.N. Fry, R. Sayaman, M.H. Dickinson, The aerodynamics of free-flight maneuvers in Drosophila, Science 5618 (300) (2003) 495, https://doi.org/10.1126/science.1081944.
[25] T.B. Moeslund, A. Hilton, V. Krüger, A survey of advances in vision-based human motion capture and analysis, Comput. Vis. Image Understanding 2–3 (104) (2006) 90, https://doi.org/10.1016/j.cviu.2006.08.002.
[26] T.L. Hedrick, Software techniques for two- and three-dimensional kinematic measurements of biological and biomimetic systems, Bioinspiration Biomimetics 3 (3) (2008) 34001, https://doi.org/10.1088/1748-3182/3/3/034001.
[27] T. Zhang, J. Liu, S. Liu, C. Tang, P. Jin, A 3D reconstruction method for pipeline inspection based on multi-vision, Measurement (98) (2017) 35–48, https://doi.org/10.1016/j.measurement.2016.11.004.
[28] C. Kuang, D. Luo, X. Liu, G. Wang, Study on factors enhancing photobleaching effect of fluorescent dye, J. Meas. 4 (46) (2013) 1393, https://doi.org/10.1016/j.measurement.2012.11.039.
[29] F. Tauro, C. Pagano, M. Porfiri, S. Grimaldi, Tracing of shallow water flows through buoyant fluorescent particles, Flow Meas. Instrum 26 (Suppl. C) (2012) 93, https://doi.org/10.1016/j.flowmeasinst.2012.03.007.
[30] A. Shishkin, P. Schützner, C. Wagner, F.-O. Lehmann, Experimental quantification and numerical simulation of unsteady flow conditions during free flight maneuvers of insects, in: Nature-Inspired Fluid Mechanics, Springer, Berlin Heidelberg, 2012, p. 65.
[31] Y.I. Abdel-Aziz, H.M. Karara, Direct linear transformation into object space coordinates in close-range photogrammetry, Symposium on Close-Range Photogrammetry, (1971) 1–18.
[32] H. Wagner, Flight performance and visual control of flight of the free-flying housefly (Musca Domestica L.) I. Organization of the flight motor, Philos. Trans. Roy. Soc. Lond. B 1158 (312) (1986) 527, https://doi.org/10.1098/rstb.1986.0017.
[33] W. Stark, M.A. Johnson, Microspectrophotometry of Drosophila visual pigments: determinations of conversion efficiency in R1–6 receptors, J. Comp. Physiol. 4 (140) (1980) 275, https://doi.org/10.1007/bf00606268.
[34] A. Lee, VirtualDub video capture/ processing utility (Version 1.9.9), (2009). http://www.virtualdub.org.
[35] J. Chapman, D. Goulson, Environmental versus genetic influences on fluctuating asymmetry in the house fly, Musca domestica, Biol. J. Linn. Soc. 3 (70) (2000) 403, https://doi.org/10.1111/j.1095-8312.2000.tb01231.x.
[36] T. Haslwanter, Mathematics of three-dimensional eye rotations, Vision Res. 12 (35) (1995) 1727, https://doi.org/10.1016/0042-6989(94)00257-m.
[37] H. Wang, L. Zeng, H. Liu, C. Yin, Measuring wing kinematics, flight trajectory and body attitude during forward flight and turning maneuvers in dragonflies, J. Exp. Biol. 4 (206) (2003) 745, https://doi.org/10.1242/jeb.00183.
[38] J. Herráez, J.L. Denia, P. Navarro, J. Rodríguez, M.T. Martín, Determining image distortion and PBS (point of best symmetry) in digital images using straight line matrices, J. Meas. 91 (Suppl. C) (2016) 641, https://doi.org/10.1016/j.measurement.2016.05.051.
[39] L. Ristroph, G.J. Berman, A.J. Bergou, Z.J. Wang, I. Cohen, Automated hull reconstruction motion tracking (HRMT) applied to sideways maneuvers of free-flying insects, J. Exp. Biol. 9 (212) (2009) 1324, https://doi.org/10.1242/jeb.025502.
[40] S. Chen, Y. Dai, X. Peng, S. Li, Error analysis and surface reconstruction for swing arm profilometry, J. Meas. 87 (Suppl. C) (2016) 1, https://doi.org/10.1016/j.measurement.2016.03.004.
[41] J.P. Scholz, J.P. Millford, Accuracy and precision of the PEAK performance technologies motion measurement system, J. Motor Behav. 1 (25) (1993) 2, https://doi.org/10.1080/00222895.1993.9941634.
[42] F.-O. Lehmann, S. Pick, The aerodynamic benefit of wing–wing interaction depends on stroke trajectory in flapping insect wings, J. Exp. Biol 8 (210) (2007) 1362, https://doi.org/10.1242/jeb.02746.
[43] C.N. Balint, M.H. Dickinson, Neuromuscular control of aerodynamic forces and moments in the blowfly, Calliphora vicina, J. Exp. Biol. 22 (207) (2004) 3813, https://doi.org/10.1242/jeb.01229.
[44] E.I. Fontaine, F. Zabala, M.H. Dickinson, J.W. Burdick, Wing and body motion during flight initiation in Drosophila revealed by automated visual tracking, J. Exp. Biol 9 (212) (2009) 1307, https://doi.org/10.1242/jeb.025379.
[45] G.J. Berman, Z.J. Wang, Energy-minimizing kinematics in hovering insect flight, J. Fluid Mech. 582 (2007), https://doi.org/10.1017/s0022112007006209.

[46] T. Engels, D. Kolomenskiy, K. Schneider, F.-O. Lehmann, J. Sesterhenn, Bumblebee flight in heavy turbulence, Phys. Rev. Lett. 2 (116) (2016), https://doi.org/10.1103/PhysRevLett. 116.028103 028103.
[47] W. Shyy, Y. Lian, J. Tang, H. Liu, P. Trizila, B. Stanford, L. Bernal, C. Cesnik, P. Friedmann, P. Ifju, Computational aerodynamics of low Reynolds number plunging, pitching and flexible wings for MAV applications, Acta Mech. Sin. 4 (24) (2008) 351, https://doi.org/10.1007/s10409-008-0164-z.
[48] S.P. Sane, M.H. Dickinson, The aerodynamic effects of wing rotation and a revised quasi-steady model of flapping flight, J. Exp. Biol. 8 (205) (2002) 1087.
[49] S.M. Walker, A.L.R. Thomas, G.K. Taylor, Deformable wing kinematics in the desert locust: how and why do camber, twist and topography vary through the stroke?, J R. Soc. Interface 6 (2008) 734–747, https://doi.org/10.1098/rsif.2008.0435.
[50] A.R. Ennos, Mechanical behaviour in torsion of insect wings, blades of grass and other cambered structures, Proc. R. Soc. Lond. B 1354 (259) (1995) 15, https://doi.org/10.1098/rspb.1995.0003.
[51] G.C.H.E. de Croon, M. Perçin, B.D.W. Remes, R. Ruijsink, C. De Wagter, The DelFly: Design, Aerodynamics, and Artificial Intelligence of a Flapping wing robot, first ed., Springer, 2015.
[52] C. Richter, H. Lipson, Untethered hovering flapping flight of a 3d-printed mechanical insect, Artif. Life 17 (2) (2011) 73–86, https://doi.org/10.1162/artl_a_00020.
[53] F. van Breugel, Z. Ern Teoh, H. Ern Teoh, in: D. Floreano, J.-C. Zufferey, M.V. Srinivasan, C. Ellington (Eds.), A passively stable hovering flapping micro-air vehicle, Springer, Berlin Heidelberg, 2010, p. 171.
[54] F. van Breugel, W. Regan, H. Lipson, From insects to machines, Robot. Autom. Mag. IEEE 4 (15) (2008) 68, https://doi.org/10.1109/mra.2008.929923.
[55] P. Zdunich, D. Bilyk, M. MacMaster, D. Loewen, J. DeLaurier, R. Kornbluh, T. Low, S. Stanford, D. Holeman, Development and testing of the mentor flapping-wing micro air vehicle, J. Aircraft 5 (44) (2007) 1701, https://doi.org/10.2514/1.28463.